Journal of Physics: Conference Series

PAPER • **OPEN ACCESS**

Cryogenic quenching process enhancement through coating and microstructure optimization

To cite this article: Marco Graffiedi *et al* 2024 *J. Phys.: Conf. Ser.* **2766** 012139

Journal of Physics: Conference Series **2766** (2024) 012139 doi:10.1088/1742-6596/2766/1/012139

Cryogenic quenching process enhancement through coating and microstructure optimization

Marco Graffiedi[1], Francis J. Dent[2], Sepideh Khodaparast[2] and Matteo Bucci[1]

1 Nuclear Science and Engineering, Massachusetts Institute of Technology, Cambridge 02139, US

2 School of Mechanical Engineering, University of Leeds, LS2 9JT Leeds, UK

E-mail: mgraff@mit.edu

Abstract. In this work, we explore the impact of coatings and microstructures on heat transfer during a cryogenic quenching process. An easily reproducible quenching test is presented as a benchmark for testing different solutions. The study involves two different flat polymeric coatings as well as three porous microstructures. The results show that pairing a low-conductive coating with an appropriate porous surface microstructure on top of a stainless-steel plate can reduce the chill down time, accelerating the transition from room temperature to liquid nitrogen temperature, by a factor of five. High speed video recordings have been used to analyse the quenching process with different coatings and microstructures showing how the suppression of the film boiling regime is the key to enhancing the quenching process.

1. Introduction

Managing cryogenic fluids poses significant challenges. In particular, when a cryogenic fluid is (1) transferred between two tanks, (2) sent to a rocket engine, or (3) used as a coolant, it is typically required that the flow is stable and with no vapor [1]. Since cryogenic piping, tanks, and equipment are generally at a higher temperature than the saturation temperature of the fluid, during the liquid transfer vigorous, while the equipment cools down, the liquid vaporizes vigorously. This process, called chill-down, consists of three stages: (1) film boiling, (2) transition boiling, and (3) nucleate boiling [2]. In almost all applications, the vaporized cryogen, along with entrained liquid droplets, is vented into the environment or outer space. Thus, the design of the transfer line and the procedure of chill-down should focus on minimizing the fluid loss.

Enhancing the chill-down process has been a challenging yet intriguing endeavor for researchers and inventors. Chung et al. demonstrated the efficacy of low conductivity coatings in cryogenic chill-down [3]. Other researchers have shown that the roughness has limited effect on the Leidenfrost temperature [4] and that nano-porous surfaces can increase the Leidenfrost temperature and the critical heat flux [5]. The present study will focus on accelerating the chill-down process by early suppression of the film boiling regime using low conductivity coatings in combination with surface microstructures.

2. Method

2.1 Experimental apparatus

The experimental apparatus is made by a 2-layers reservoir that is continuously filled with liquid nitrogen. The reservoir is insulated with Styrofoam and has a penetration on the bottom featuring a 4mm internal diameter tubing which acts as a nozzle, see figure 1. The jet of liquid nitrogen, when not interacting with the specimen, is collected in a small dewar positioned below the experiment. The specimen is mounted on a movable support and translated to make contact with the liquid jet when the flow is fully developed.

2.2 Measurement system and accuracy

Three thermocouples are spot-welded on the back of the 0.9 mm thick stainless-steel specimen, one at the center of the specimen and two at 15 mm distance from the center, see figure 2. Each thermocouple is calibrated with a two-points calibration between room temperature (293 K) and liquid nitrogen temperature (77.3 K), which leads to an accuracy of $\pm$ 2.4K. The three thermocouples are recorded with an acquisition rate of 275 Hz. The quenching process is also recorded using a high-speed camera with a framerate of 550 fps.

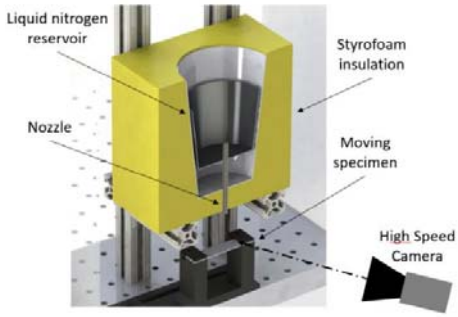

Figure 1. CAD rendering of the experimental apparatus (cross-section).

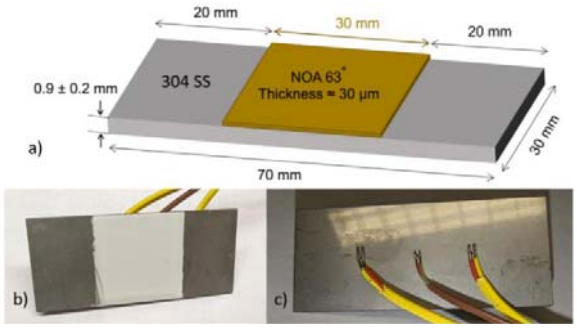

Figure 2. a) Specimen dimensions. b) Front picture (the surface coated looks white-ish). c) Rear picture with spot-welded thermocouples.

2.3 Coatings and microstructures tested

Identical stainless-steel substrates have been used to test two different flat polymeric coatings as well as three porous microstructures. The 2 polymeric coatings used are the Norland Optical Adhesive 63 (NOA63 or C63) and the Norland Optical Adhesive 68 (NOA68 or C68).

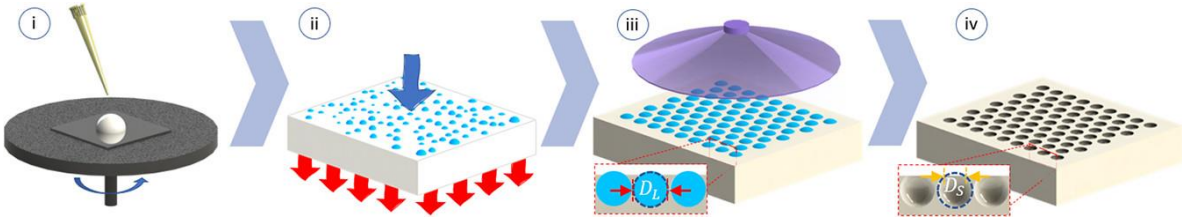

Figure 3. Schematic showing the main steps in the temporally arrested breath figure methodology. (i) Spin coating of the polymer. (ii) Condensation of water droplet on the surface. (iii) Droplets grow is arrested by UV curing. (iv) During curing, water droplets will evaporate.

Three different microstructures have been manufactured on the coating by Temporally Arrested Breath Figure (TABF) process. The TABF starts from coating the liquid polymer by spin coating (figure 3.i) and by cooling the specimen in a controlled environment using a Peltier cell. The cooling is used to induce condensation of water droplets which displace the polymer adhesive creating spherical footprints on the coating itself (figure 3.ii). The curing of the polymer by UV irradiation is used to arrest the growth of the pattern and solidify the polymer coating (figure 3.iii). After the complete curing of the adhesive, the droplets are evaporated by heating the surface (figure 3.iv) [6,7]. The parameters that characterize the coatings are pores density N_d and pore diameter D_S, as defined in figure 3. The three different microstructures tested are called Highly Packed Large (HPL), Highly Packed Small (HPS), and Spatially Modulated (SM). The properties and microscope pictures of these microstructures are summarized in table 1 and in figure 4.

Table 1. Characteristics of the microstructure tested. In particular, pores density $\boldsymbol{N_d}$, and pores diameter $\boldsymbol{D_S}$.

MICRO STRUCTURE	Base Material	N_d $[10^3 m^{-2}]$	D_S [μm]
HPL	C68	6	9 ± 2
HPS	C68	56	2.5<
SM	C63	7	6 ± 1

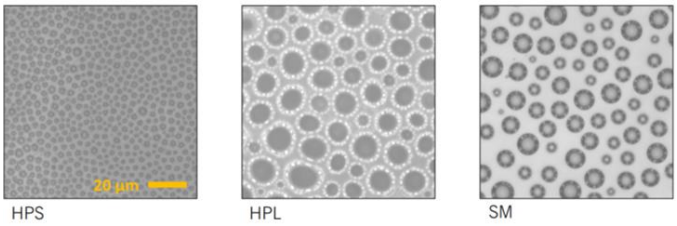

Figure 4. Optical microscope pictures of the pores in the solid films.

3. Method

3.1 Inverse problem

Since the measurement of the temperature is done on the back, an inverse thermal problem needs to be solved to calculate the temperature on the specimen surface. By using the analytical solution provided by Burggraf [8], it is possible to calculate the temperature on the top surface of the stainless-steel plate $T(\delta, t)$ and the heat flux at the interface between the stainless-steel sample and the coating $q_\delta(t)$ by knowing how the temperature on the bottom surface changes in time $T_0(t)$; see figure 5 for reference. Then, we computed the temperature at the top of the coating $T_W = T_\delta + \frac{q_\delta(t)}{k_c}\delta_c$, where k_c and δ_c are the thermal conductivity and the thickness of the coating, respectively. Results are shown in the bottom plot in figure 6.

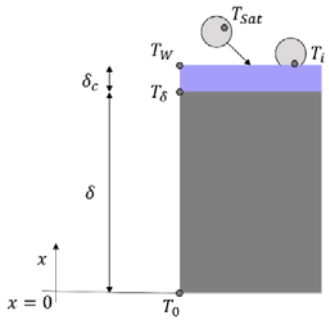

Figure 5. Schematic for the inverse problem and rewetting temperature calculation.

Since the microstructure introduces voids in the coating, the effective thermal resistance R_p of the microstructure has to be modeled, see figure 6 for reference. This is done by integrating the infinitesimal thermal resistance dR_p layer by layer as in Eq.1, where the meaning of the geometrical quantities is showed in figure 6:

$$R_p = \frac{(\mathrm{T}_c - \mathrm{T}_\mathrm{p})}{q''} = \int_0^{R_p} dR_p = \int_0^h \frac{dR_p}{dz} dz = \int_0^h \frac{1}{k\{1 - [R^2 - (h - R - z)^2]\pi N_d\}} dz. \quad (1)$$

In conclusion, the wall temperature becomes $T_c = T(\delta, t) + q_\delta(t)\left(\frac{\delta_c - h}{k_c} + \frac{1}{R_p}\right)$.

4. Results and modelling

4.1 Results of the inverse problem

In figure 6, the temperature evolutions and boiling curves for all the different tests have been plotted. Notably, the use of C68 or C63 coatings reduces the chill-down time to approximately 1/3rd respect to the case without coating. A similar result has been showed by Chung [3] using a 0.5mm thick stainless-steel pipe coated with Teflon in internal flow.

As it can be seen from the images S1, S2, and SM1 in figure 6, at high surface temperature the heat transfer regime is film boiling, and there is no intimate contact between the liquid and the surface. When the wall is cooler, the vapor film between liquid and the wall is not stable and the wall is wetted. After the wetting, higher heat fluxes are measured as shown by the points S3, SM2, and HPL1. In the case of HPL microstructure, a puddle forms right after the jet contacts the surface, see point HPL1, showing that the Leidenfrost temperature is higher than the ambient temperature.

A dedicated test has been performed for the HPL microstructure, where the specimen was pre-heated to a temperature of $400K$ in order to assess its Leidenfrost temperature. We do not report here the full quenching curve, only the Leidenfrost temperature in figure 8.

We note that the solution of the inverse problem seems to diverge in $q_\delta(t)$ near the end of the test. The most probable explanation of this phenomena is the wetting of the bottom surface of the specimen which creates a sudden and faster cooling. Considering that this "abnormal" behavior is far from the film boiling regime, it does not affect the overall quenching performance and it will not be analyzed it in the present work.

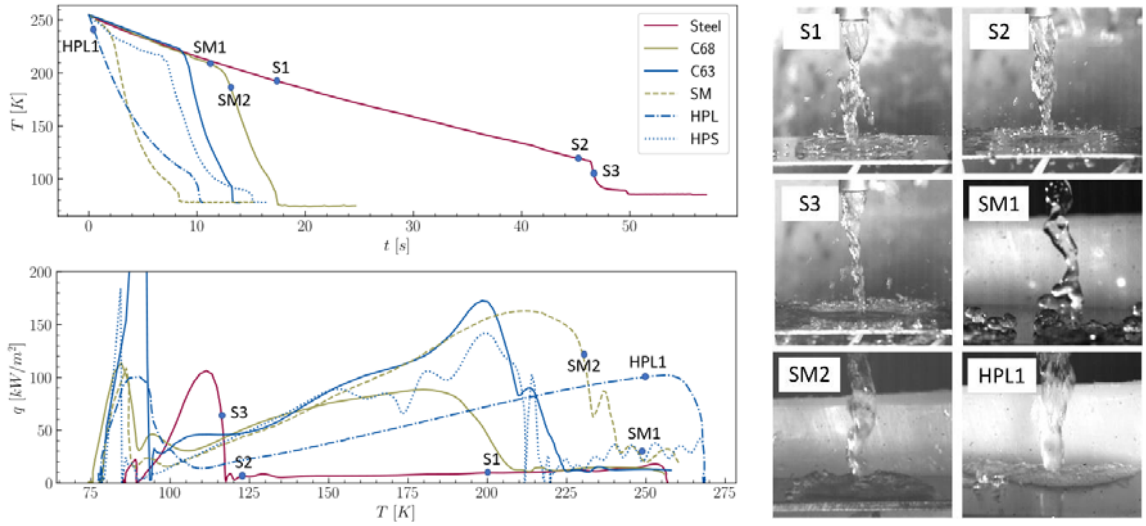

Figure 6. Comparison of the experimental results. Top plot, the temperature time evolutions. Bottom plot, the corresponding boiling curve considering q_w and T(δ,t) that are calculated using the solution to inverse problem. The figures on the right are from the high-speed video recordings.

4.2 Rewetting in the presence of coatings

As shown in figure 6, the presence of the coatings C63 and C68 anticipate the wetting of the surface. We here propose a model where the surface can be wetted when the contact temperature between the liquid and the solid is below the critical value of $T_l = 104K$, which is fairly close to the one that is predicted by the

empirical formulation proposed by Sakurai [9]. Then, we can calculate the wall temperature T_{rew} that would permit the wetting as

$$T_{rew} = \frac{T_I(\varepsilon_w + \varepsilon_{LN2}) - \varepsilon_{LN2} T_{LN2}}{\varepsilon_w}, \quad (2)$$

where ε_W is the effusivity of the top layer material, ε_{LN2} the effusivity of liquid nitrogen, and T_{LN2} the temperature of the liquid nitrogen. It is interesting to note that, in case of low effusivity coatings, the thickness of the coating matters. Thus, we expect this formulation to be valid if the thickness of the coating is larger than the thermal penetration length $\delta_p = 2.3\sqrt{\alpha_W \tau}$ [10], calculated considering a bubble characteristic life-time of $\tau = 1\ ms$ and the diffusivity of the top layer material α_W. This limitation is necessary to avoid secondary effect due to the thermal interaction of the boiling process with the high-effusivity bulk material. This hypothesis will be verified by testing coatings with different thicknesses in a future work.

4.3 Rewetting in the presence of microstructures

In case of microstructures on the surface, like in figure 7, we will consider effective conductivity $k_{eff}(z) = kS_s(z)$ and density $\rho_{eff}(z) = \rho S_s(z)$ of the microstructure, where $S_s(z)$ is the solid fraction at the depth z; In particular, we will consider the solid fraction of the top surface as $S_s(0) = 1 - r_0^2 \pi N_d$ and the corresponding effective effusivity as $\varepsilon_{eff} \approx \varepsilon S_s(0)$. Thus, the T_{rew} can then be calculated using (2). The results of this approach are compared with the experimental results in figure 8.

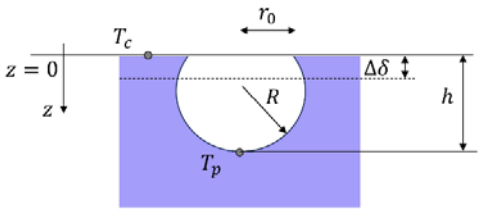

Figure 7. Schematic to characterize the microstructure.

As shown in figure 8, it seems that Eq. (2) captures the behavior of the coatings and the microstructures SM and HPL. However, data for HPS seems not to follow the same trend as SM and HPL. The reason behind may be tied to the very small depth of the HPS microstructure, which is one order of magnitude lower than the δ_p. However, we cannot exclude hydrodynamics effects in this analysis. In particular, we could observe a similarity between the HPS microstructure and the work of Del Cerro et al. [11] where micropatterned surface seems to reduce the Leidenfrost Point for water droplets.

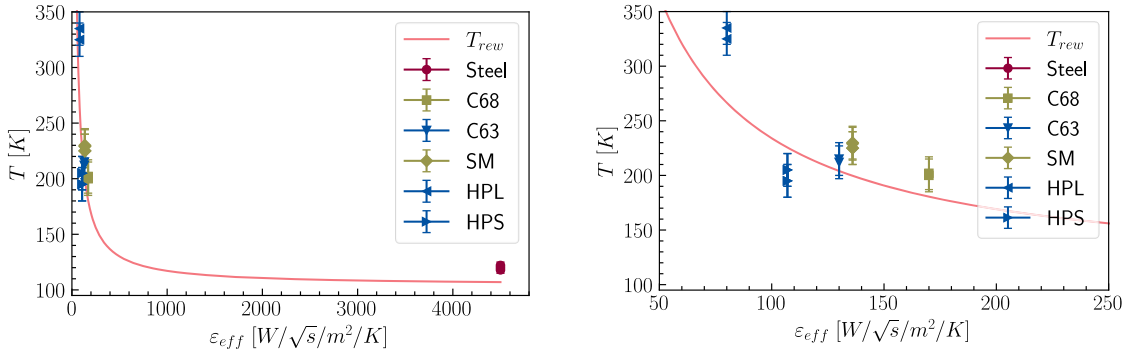

Figure 8. Comparison of the experimental results with the proposed formulation for the rewetting temperature of the wall.

5. Conclusions

In this work, we showed that using a low-conductive coating with appropriate porous surface microstructures on top of a stainless-steel plate can lead to an early suppression of the film boiling regime, promoting the wetting of the surface, and reducing the chill-down time with cryogenic fluids by a factor of five. We proposed a simple theory to explain the raise of the Leidenfrost temperature by starting from first principles and existing literature. In conclusion, the work suggests that the effective thermal effusivity of the top layer is a key factor in determining the wetting temperature. Moreover, this effect seems limited by the penetration length of the thermal perturbation due to nucleate boiling on the surface. To further corroborate these two strong hypotheses, we are planning further experiments to test the limit of the penetration length as well as the generality of the model for porous coatings.

References

[1] Hartwig J and Vera J 2016 Numerical modeling of the transient chilldown of a cryogenic propellant transfer line *J Thermophys Heat Trans* **30** 2
[2] Brennan JA, Brentari EG, Smith R V and Steward WG 1966 Cooldown of Cryogenic Transfer Lines an Experimental Report *Legacy CDMS NASA*
[3] Chung JN, Darr SR, Dong J, Wang H and Hartwig JW 2020 Heat transfer enhancement in cryogenic quenching process *International Journal of Thermal Sciences* **147**
[4] Li Z, Yu D, Cui J, Feng P and Feng F 2021 Influences of Brass Surface Morphology on Leidenfrost Effect during Liquid Nitrogen Cooling *Applied Sciences* **11** 10323
[5] Hu H, Xu C, Zhao Y, Shaeffer R, Ziegler KJ and Chung JN 2015 Modification and enhancement of cryogenic quenching heat transfer by a nanoporous surface *Int J Heat Mass Transf* **80**
[6] Dent FJ, Harbottle D, Warren NJ and Khodaparast S. 2022 Temporally Arrested Breath Figure *ACS Appl Mater Interfaces* **14** 23
[7] Dent FJ, Harbottle D, Warren NJ and Khodaparast S. 2023 Exploiting breath figure reversibility for in situ pattern modulation and hierarchical design *Soft Matter* **19**
[8] Burggraf OR 1964 An Exact Solution of the Inverse Problem in Heat Conduction Theory and Applications *J Heat Transfer* 1964 **86** 373
[9] Sakurai A, Shiotsu M and Hata K 1990 Effects of system pressure on minimum film boiling temperature for various liquids *Exp Therm Fluid Sci* **3** 4
[10] Bergman TL, Lavine PD and Incropera FP 2018 *Fundamentals of Heat and Mass Transfer* (John Wiley & Sons)
[11] Del Cerro A, Marín ÁG, Römer GRBE, Pathiraj B, Lohse D and Huis AJ 2012 Leidenfrost point reduction on micropatterned metallic surfaces *Langmuir* **28** 42